Desalination and Water Treatment
www.deswater.com

doi: 10.5004/dwt.2019.23565

143 (2019) 323–332
March

Isotherm, kinetics and thermodynamics of methylene blue dye adsorption onto CO_2-activated pyrolysis tyre powder

Mohd Shafiq Hakimi Mohd Shaid[a,b], Muhammad Abbas Ahmad Zaini[a,b,*], Noor Shawal Nasri[b,c]

[a]*Centre of Lipids Engineering & Applied Research (CLEAR), Ibnu-Sina Institute for Scientific & Industrial Research, Universiti Teknologi Malaysia, 81310 UTM Johor Bahru, Johor, Malaysia, email: abbas@cheme.utm.my (M.A.A. Zaini)*
[b]*School of Chemical & Energy Engineering, Faculty of Engineering, Universiti Teknologi Malaysia, 81310 UTM Johor Bahru, Johor, Malaysia*
[c]*UTM-MPRC Institute for Oil & Gas, Universiti Teknologi Malaysia, 81310 UTM Johor Bahru, Johor, Malaysia*

Received 27 March 2018; Accepted 2 December 2018

ABSTRACT

This work was aimed at evaluating the adsorption properties of methylene blue dye by CO_2-activated pyrolysis tyre powder carbons. The activated carbons were prepared under the flow of CO_2 at temperatures between 900°C and 1,000°C for durations of 2–8 h. Consequently, the activated carbons were characterized for textural properties, pH_{PZC}, surface functional groups, and surface morphology. Batch adsorption was conducted by varying the concentrations of methylene blue and contact times, from which the experimental data were fitted into isotherm and kinetic models. Results show that CO_2 activation at 1,000°C for 2 h yields a 57.2% activated carbon with a 243 m^2/g specific surface area and a maximum methylene blue adsorption capacity of 132 mg/g. The Langmuir and Redlich–Peterson models appeared to fit the equilibrium data well. The rate of adsorption data obeyed the pseudo-second-order kinetic model, while the rate-limiting step in the adsorption of methylene blue is probably film diffusion. The adsorption is endothermic and spontaneous with increasing temperature. Activated carbon prepared from pyrolysis tyre powder by CO_2 activation is a promising candidate to abate dye wastewater pollution.

Keywords: Activated carbon; CO_2 activation; Isotherm; Kinetics; Thermodynamics; Pyrolysis tyre powder

1. Introduction

Dyes are broadly used in printing materials, fabrics, textiles, cosmetics, plastics, papers, and foods [1–3]. Globally, 7×10^5 tons of more than 0.1 million types of dyes are manufactured annually [4]. Unfortunately, the dyes eventually end-up as industrial wastes, and consequently are discharged into the water bodies in the form of colored wastewater. The colored wastewater leads to the aesthetic pollution, prevent the penetration of sunlight and further upsetting the marine ecosystem and growth rate of aquatic living creatures, and food chains as a result of decreasing oxygen content due to the inhibition of photosynthesis of aquatic plants [5,6]. Also, excessive exposure to dye may cause increased heart rate, vomiting, shock, jaundice, quadriplegia, cyanosis, tissue necrosis, skin reaction, and cancer [7,8].

A number of treatment strategies including that of physical, chemical, and biological methods have been applied to dye-containing wastewater [9]. Of these, adsorption is a preferred technique because of several advantages, namely simple and easy to operate, inexpensive, ease of accessibility to a variety of adsorbents, high efficiency, and negligible by-product, thus an

* Corresponding author.

environmental friendly process [10–12]. Adsorption is an effective treatment process to remove various pollutants in water even at lower concentration. Activated carbon is a commonly used adsorbent for dye adsorption [13,14]. The state-of-the-art research on activated carbon has intensified over the years, in response to the competitive pursuits in finding eco-friendly and low-cost solutions to treat wastewater from several industrial sectors.

Each year, scrap tyres are discarded in huge bulks to the environment in a staggering amount of 1.5 billion [15]. The trend of discarding the unwanted tyres is consistent across the city-status townships [16]. Typically, two strategies are chosen to deal with scrap tyres – disposing and recycling. Through a conventional disposal strategy, the scrap tyres are either incinerated at high temperatures or buried in landfills. However, the disposal strategy often results in polluting the natural environment, hence impacting the public health. For instance, lands filled with the used tyres may eventually become the sites for flies and mosquitoes to breed and thrive, while the incineration of scrap tyres releases greenhouse gases that are also the causal factors of cancer [17,18]. Hence, the recycling of scrap tyres is seen as a sustainable solution to overcome the above-mentioned issues.

The scrap tyres are recycled to create new products and to generate energy [19]. For instance, they are milled and blended to strengthen the concrete structures owing to their unique physical characteristics; light weight, easily drained and compressed, and retain heat well. In energy generation, pyrolysis of spent tyres is a process that allows fuel of inferior quality to be produced. Recovering energy from wastes maximizes the profitability, reduces the release of toxic gases, and allows the energy to be integrated in-house [20]. However, the pyrolysis process itself inevitably produces a by-product in the form of fine carbon powder, known as pyrolysis tyre powder. It is envisioned that the solid residue would be a promising precursor of activated carbon, which later could be used to treat various water pollutants such as dyes and heavy metals. Previous studies reported the chemical activation of pyrolysis tyre powder to remove dyes from water [21,22]. However, it should be noted that the residue is already rich in carbon content as it already undergone a pyrolysis process, hence the chemical activation and pre-carbonization may not be necessary in the activated carbon preparation. The present work was aimed to evaluate the physical activation of pyrolysis tyre powder using CO_2 at different activation times and temperatures. Methylene blue dye was utilized as a model pollutant to probe the adsorption performance. Isotherm, kinetic and thermodynamic models were used to analyze the adsorption data.

2. Materials and methods

2.1. Materials

The pyrolysis waste tyre powder (WTP) was obtained from a brick factory in Johor state of Malaysia. The vessel of CO_2 gas for activation was supplied by Mega Mount Gases (Malaysia). Methylene blue dye powder ($C_{16}H_{18}N_3SCl$, 319.9 g/mol) for batch adsorption studies was purchased from QReC (Malaysia). All chemicals are of analytical grade and were used as received.

2.2. Preparation and characterization of activated carbon

Activated carbons were derived from WTP by physical activation using CO_2. The desired mass of WTP was added on a ceramic boat, and was placed at the centre of a tubular furnace. A flow of CO_2 was introduced into the furnace for 10 min to prevent oxygen from initiating the combustion during activation. Activated carbons were prepared at temperatures of 900°C and 1,000°C for durations of 2–8 h. Table 1 summarizes the designation of activated carbons prepared by CO_2 activation.

The WTP was characterized for oil content and ash content. The oil content was determined by dividing the mass of oil with the original mass of WTP before extraction. The oil was extracted by refluxing hexane using a Soxhlet unit, and the recovery of oil and solvent was performed using a rotary evaporator. The ash content was determined by subjecting WTP in a muffle furnace at temperature of 850°C for 2 h. The ash content was calculated by dividing the residual mass (left-over) with the initial mass of WTP. The thermal degradation profile of WTP was obtained using a TGA 4000 (PerkinElmer, USA) at a N_2 flow of 40 mL/min and a heating rate of 10°C/min from room temperature to 900°C.

Activated carbons were characterized for yield, textural properties, surface functional groups, pH_{PZC} and surface morphology. The yield was calculated by dividing the mass of activated carbon with the initial mass of WTP. The pH of point zero charge (pH_{PZC}) is defined as the pH at which the net surface charge is equal to zero. A hundred milligrams of activated carbon were brought into contact with 0.1 M NaCl solution of varying initial pH, and the mixture was allowed to equilibrate for 24 h. The pH_{PZC} is determined when the final pH is equal to the initial pH. The specific surface area of activated carbon was obtained using a PulseChemisorb 2705 analyzer (Micrometrics, USA). The surface morphology of activated carbon was elicited via a TM3000 scanning electron microscope (Hitachi, Japan). A PerkinElmer FTIR spectrometer was used to evaluate the chemical bonds and functional groups on the surface of activated carbon.

2.3. Batch adsorption studies

Thirty milligrams of activated carbon were added into a flask containing 30 mL of methylene blue dye (MB) solution of varying concentrations between 5 and 200 mg/L, and the solution pH was not adjusted. For the effect of solution pH on MB adsorption, few drops of 0.5 M NaOH and 0.5 M NaOH were used to adjust the solution pH. The mixture was allowed to equilibrate at ambient temperature for

Table 1
Designation of activated carbons

Activating temperature (°C)	Activating time (h)	Designation
900	2	AC9-2
900	5	AC9-5
900	8	AC9-8
1,000	2	AC10-2
1,000	5	AC10-5

72 h. The concentration of MB was analyzed using a Drawell UV–Vis spectrophotometer (DU-8200) at a wavelength of 620 nm (R^2 = 0.9995). The adsorption capacity, Q_e (mg/g), was calculated as:

$$Q_e = \frac{V(C_o - C_e)}{M} \tag{1}$$

where V (L) is the volume of MB solution, M (g) is the mass of activated carbon, C_o and C_e (mg/L) are the initial and equilibrium concentrations, respectively [23].

The equilibrium data were analyzed using three empirical equations, that is, Langmuir, Freundlich, and Redlich–Peterson models. The Langmuir model is given as follows:

$$Q_e = \frac{Q_m b C_e}{\left(1 + bC_e\right)} \tag{2}$$

where Q_m (mg/g) represents the maximum adsorption capacity and b (L/mg) is the Langmuir constant which reflects the adsorption energy and the site binding affinity. The Langmuir isotherm assumes that the adsorption takes place over a homogeneous adsorbent surface with a single layer coverage [24]. The Freundlich model is expressed as follows:

$$Q_e = K_f C_e^{1/n} \tag{3}$$

where K_f ((mg/g)(L/mg)$^{1/n}$) is the Freundlich isotherm constant attributed to the adsorption capacity, and n is the empirical parameter of adsorption intensity. The Freundlich isotherm assumes that the adsorption takes place over a heterogeneous surface with a multilayer coverage [6]. The Redlich–Peterson (R–P) model is expressed as follows:

$$q_e = \frac{KC_e}{\left(1 + a.C_e^{\,g}\right)} \tag{4}$$

where K (L/g) and a represent the R–P isotherm constants, and g is a booster that falls between zero and one. This model is a hybrid featuring both Langmuir and Freundlich models, and is applicable for a wide range of concentration, either for homogeneous or heterogeneous system [25].

Two selected activated carbons were evaluated for the rate of adsorption at concentrations of 5, 15 and 20 mg/L. Thirty milligrams of activated carbon was brought into intimate contact with 30 mL of MB solution of known concentrations. The residual concentration was measured at various time intervals. The adsorption capacity at time, t, was computed as follows:

$$Q_t = \frac{V(C_o - C_t)}{M} \tag{5}$$

where Q_t (mg/g) is the dye adsorption at time t, and C_t (mg/L) is the dye concentration in the solution at time t [26].

The kinetics data were analyzed using kinetics models, namely pseudo-first-order, pseudo-second-order, and intraparticle diffusion as expressed in Eqs. (6)–(8), respectively [27,28].

$$Q_t = Q_e\left[1 - \exp\left(-k_1 t\right)\right] \tag{6}$$

$$Q_t = \frac{k_2 Q_e^2 t}{\left(1 + k_2 Q_e t\right)} \tag{7}$$

$$Q_t = k_d t^{1/2} + c \tag{8}$$

where k_1 (min^{-1}) is the pseudo-first-order rate constant, k_2 (g/mg min) is the pseudo-second-order rate constant, k_d (mg/g min$^{0.5}$) is the intraparticle diffusion rate constant, and c (mg/g) represents the y-intercept of intraparticle diffusion plot. The pseudo-first-order model assumes that the rate of physical adsorption (physisorption) increases with increasing the removal capacity of solute, and that the external diffusion is significant. The pseudo-second-order model is based on the assumption that the ion exchange and/or covalent forces promote the electron sharing and exchanging (chemisorption) between the adsorbent and solute. On the other hand, the intraparticle diffusion model allows the diffusing mechanisms to be identified [29].

Adsorption thermodynamics was carried out by varying the process temperatures between 30°C and 50°C to evaluate the reversible and spontaneous nature of the adsorption process [30]. The Gibbs energy ($\Delta G°$), enthalpy ($\Delta H°$), and entropy ($\Delta S°$) were computed by the van't Hoff equation as follows:

$$\ln K_d = \frac{\Delta S^o}{R} - \frac{\Delta H^o}{RT} \tag{9}$$

$$K_d = \frac{C_{Ae}}{C_e} \tag{10}$$

where K_d is the distribution constant and C_{Ae} (mg/L) is the concentration of dye on the activated carbon at equilibrium [31].

3. Results and discussion

3.1. Characteristics of activated carbon

The oil content and ash content of pyrolysis tyre powder (WTP) are 5.02% and 22.4%, respectively. The thermogravimetric analysis as displayed in Fig. 1 was carried out to investigate the weight loss pattern of WTP during physical activation. The ignition temperature of combustion and decomposition is initiated at around 600°C–700°C, while the burnout temperature is approximately 810°C. The ignition temperature is quite high compared with the common temperature to incinerate the waste tyre, ca. 270°C. The material with ignition temperature of 550°C or lower is mostly rich in organic compounds, which are generally broken down and

eliminated during the pyrolysis of tyres. The high ignition temperature indicates that it is difficult to ignite WTP due to its high fraction of inorganic/ash content, which retards the glowing of combustion. The temperature at which the material has reached 8% weight loss is known as the burnout temperature. The burnout temperature of 810°C is higher than that of spent tyres (~500°C), attributed to a high content of inorganic matters that are incombustible [32,33].

From Fig. 1, the thermal behavior of WTP can be divided into three phases. In the first phase, a significant weight loss from room temperature to 200°C is caused by the gasification of volatile matters. In the second phase, a weight loss at temperatures between 500°C and 600°C indicates the decomposition of remaining organic compounds, including oil residue that was not fully recovered during pyrolysis. The third phase shows a sideway pattern of weight loss ranging between 600°C and 900°C, which corresponds to the combustion of fixed carbon. This phase indicates that the combustion has almost ended. A small decrease in weight of only 8% at 900°C could be attributed to the domination of fixed carbon.

Table 2 summarizes the characteristics of activated carbons. The yield of activated carbons by CO_2 activation is ranging between 32.1% and 66.2%. A longer activation time at a higher temperature often results in the collapse of pore textures due to excessive burning-off, hence decreasing the carbon yield [34]. From Table 2, AC9-5 and AC10-2 exhibit the highest specific surface area of 238 and 243 m^2/g, respectively. Obviously, the specific surface area decreases with increasing activation time (AC9-8) and temperature (AC10-5). The surface area of activated carbon is likely to diminish under heating at high temperature as a result of pores collapse [35].

Fig. 2 shows the N_2 adsorption–desorption isotherms of AC10-2, and the textural properties of AC10-2 are summarized in Table 3. The adsorption branch in Fig. 2 shows a distinctive isotherm of mesopore-rich non-porous material. It signifies the unrestricted monolayer–multilayer adsorption on the carbon surface, whereby the monolayer adsorption is dominant at low relative pressure, while the multilayer adsorption takes place at high relative pressure. The adsorbate thickness gradually increases until the condensation pressure has been reached. The pressure of the first monolayer formation is lower if the interaction between the adsorbate and adsorbent is stronger, but the monolayer and multilayer formation processes are always overlapped [36]. From Fig. 2, the desorption branch shows type H3 hysteresis that is commonly attributed to mesoporous material with particles forming slit-shaped pores (plates or edged particles such as cubes), of which the size and/or shape are not uniform. The hysteresis is generally caused by different behavior in adsorption and desorption. For pore that is formed by parallel plates, the meniscus is flat (large) and cylindrical (radius is half the distance between plates) during desorption, wherein the condensation does not take place at any relative pressure [37]. From Table 3, AC10-2 is highly mesoporous (90.3%) with average pore size of 8.68 nm.

Fig. 3 shows the SEM images of pyrolysis tyre powder and AC10-2. Obviously, the surface of the two materials is

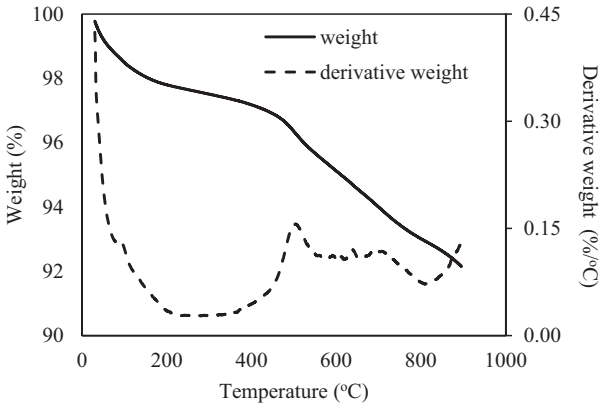

Fig. 1. Thermal degradation profile of pyrolysis tyre powder.

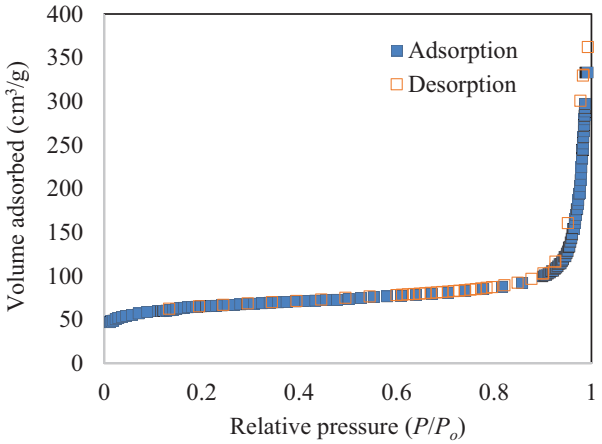

Fig. 2. N_2 adsorption–desorption isotherms of AC10-2.

Table 2
Yield, maximum adsorption capacity of methylene blue (Q_m), and specific surface area of activated carbons

Activated carbon	Yield (%)	Q_m (mg/g)	BET surface area (m^2/g)
WTP	–	–	28.4
AC9-2	66.2	46.5	97.0
AC9-5	61.5	128	238
AC9-8	55.7	86.0	204
AC10-2	57.2	132	243
AC10-5	32.1	70.7	146

Table 3
Textural properties of AC10-2

BET surface area, m^2/g	243
Micropore area, m^2/g	122
Mesopore area, m^2/g	121
Total pore volume, cm^3/g	0.514
Micropore volume, cm^3/g	0.0498
Mesopore volume, cm^3/g	0.464
Mesopore content, %	90.3
Average pore width, nm	8.68

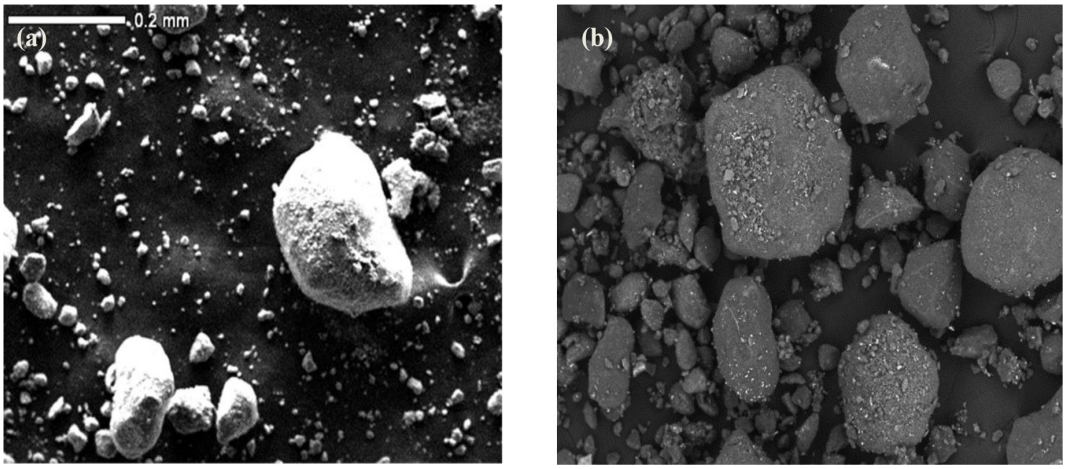

Fig. 3. SEM images of (a) pyrolysis tyre powder and (b) AC10-2.

comparable, that is, flat and non-porous. However, the latter exhibits a greater surface area of 243 m^2/g, that is nearly 8.6 times higher than the former. Upon the activation, the surface aggregate forms the slit-like pore that gives rise to pore volume and specific surface area of mesoporous AC10-2.

The pyrolysis waste tyre powder and its derived activated carbons were characterized for surface chemistry and functional groups. The presence of functional groups on the material surface is associated with the acid–base properties of activated carbon. Fig. 4 displays the FTIR spectra of pyrolysis tyre powder and AC10-2. The precursor holds several functional groups, attributed to the abundance of volatile substances. The band within the range of 3,700 cm^{-1} and above is normally assigned to physisorbed water molecules and Si–OH groups. A small peak at 3,307 cm^{-1} may be attributed to O–H stretch or N–H stretch. It infers whether the hydroxyl-containing compounds such as alcohol, phenol, and carboxylic acid are present. A small peak at 2,980 cm^{-1} is ascribed to the stretch of C–H in aliphatic chains, with the possible presence of 2-methyl-1,3-butadiene and 2-methyl-1-butane. Also, the peak at 2,350 cm^{-1} probably indicates the compensation of carbon dioxide and water in FTIR data acquisition. While, peaks at 1,775 and 1,500 cm^{-1} indicate the presence of C=O groups and C–H groups, respectively. In general, peaks at 1,400 cm^{-1} or lower are associated with the fingerprint region, which indicate the C–X bonds where X can be represented by C, N, and O. However, in some references, the peaks may also represent silicone, halogenated compounds, and sulphur stretch. Briefly, the pyrolysis waste tyre powder contains a wide range of functional groups, owing to the presence of many volatile substances [38,39].

Upon physical activation, the spectrum of activated carbon becomes more simplified. The volatiles and surface functional groups are most likely released during the activation at high temperature leading to the formation of pores. From Fig. 4(b), the intensity of absorbance decreased owing to the decreasing amount of functional groups remained on the carbon surface. Most of the peaks previously present in the raw material have been disappeared upon activation at 1,000°C. The high temperature process enhances the elimination of light and volatile matters. The new peaks assigned as, N, O, P, and Q in Fig. 4(b) represent alkenes, aromatic ring, and

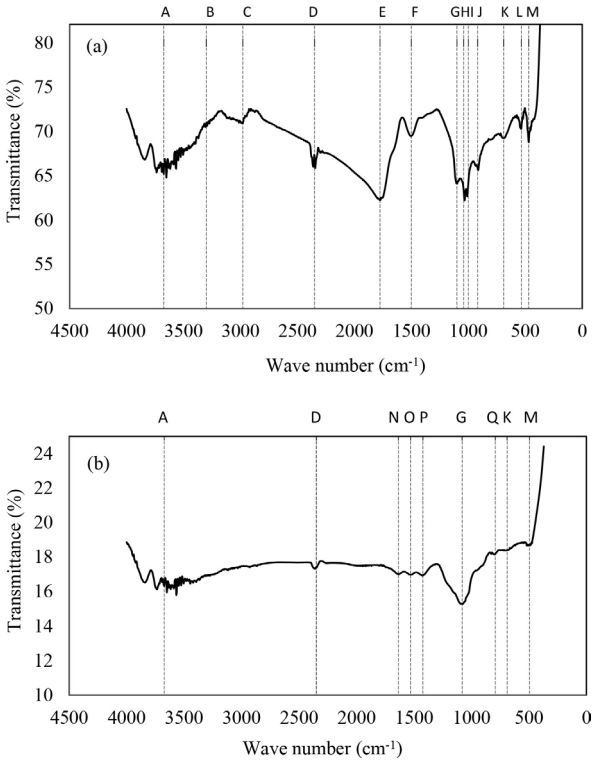

Fig. 4. FTIR spectra of (a) pyrolysis tyre powder and (b) AC10-2.

halogen compounds, signifying the development of graphitic structure of activated carbon.

Fig. 5 shows the interception point of pH_{PZC} drift curve along the 45° dashed line that represents the pH_{PZC} of AC10-2. The value was recorded as 7.0. Following this convention, the cationic dye adsorption is preferably occurred in a solution where the pH is greater than the pH_{PZC} for a negatively charged surface of activated carbon.

3.2. Equilibrium adsorption

Fig. 6 shows the adsorption of methylene blue dye (MB) onto CO_2-activated WTP carbons. In general, the adsorption

capacity, Q_e, rises as concentration increases, up until the attainment of maximum saturation. At equilibrium, the rate of adsorption is equal to the rate of desorption. The amount of Q_e is trivial at lower concentration because of a small volume of molecules restricts the adsorption capability. However, the adsorption capacity rapidly increases with increasing dye concentration, indicating a favorable, high affinity of adsorption to overcome the solid mass transfer resistance.

Fig. 7 displays the role of specific surface area of activated carbons on MB adsorption. The surface area has a positive effect on the adsorption performance of activated carbons. It can be established that the higher the surface area, the higher the interaction probabilities between the surface sites and dye molecules, hence the greater the removal capacity.

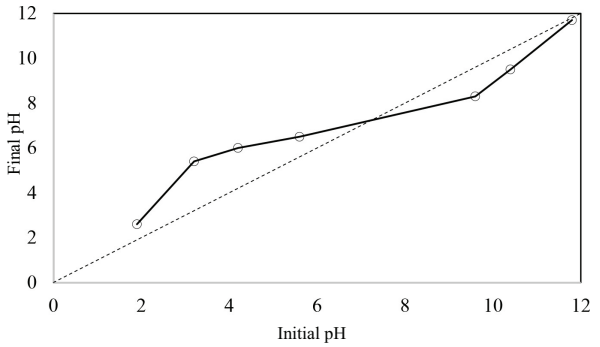

Fig. 5. pH_{PZC} of AC10-2.

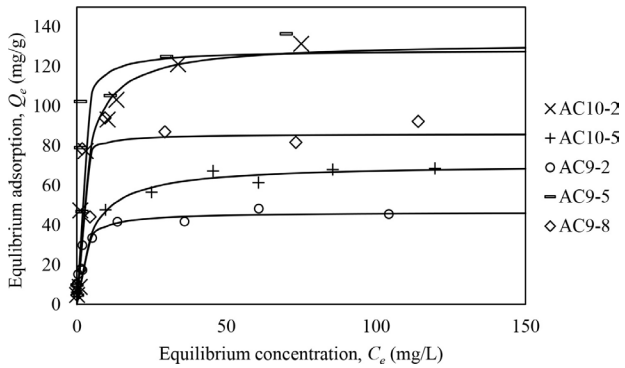

Fig. 6. Methylene blue adsorption onto activated carbons (lines were predicted by Langmuir model).

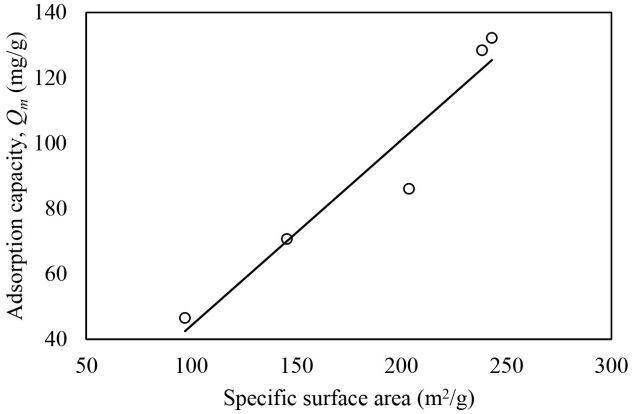

Fig. 7. Relationship between maximum uptake of methylene blue and surface area.

Table 4 summarizes the constants of isotherm models. The Langmuir model was found to better fit the equilibrium data with R^2 ranging between 0.836 and 0.989, suggesting a monolayer-type adsorption onto a homogeneous surface of activated carbon. The sum of squared errors (SSE) also supports the notion of fitted data. Besides, the n values of Freundlich model are greater than one for all activated carbons, implying an ordinary Langmuir isotherm. The Langmuir constant, b is related to the energy of adsorption. AC9-8 has the highest b, suggesting a favorable MB adsorption at low concentration. It also signifies a high affinity interaction between MB molecules and AC9-8 sites. The b constant for AC9 series shows an increasing pattern with activation temperature which could be attributed to the increase of surface reactivity of activated carbons as a result of longer activation time and exposure in CO_2, leading to the enhancement of adsorption affinity. On the other hand, a decreasing affinity of AC10 series with activation time could be associated with the decrease in surface area [40].

Fig. 8 shows the separation factor, R_L of AC10-2 at different initial concentrations of dye. The values are in the range of zero to one, signifying that the MB adsorption onto AC10-2 is favorable and reversible.

The equilibrium data of MB adsorption also satisfied the Freundlich model to a certain extent. Nevertheless, it is the least fitted model to reflect the equilibrium data as compared with Langmuir and Redlich–Peterson models. The Freundlich constant, n is linked to the adsorption intensity, whereby the $1/n$ value greater than 1 indicates a cooperative adsorption, while that lesser than 1 obeys the Langmuir isotherm. In this work, the n values are in the range of 3.51 to 14.4, accordingly the $1/n$ values are lesser than one, signifying a satisfactory fitting to Langmuir isotherm.

The adsorption data were fitted into R–P model using non-linear regression to solve for isotherm constants, namely g, a, and K [41]. In this work, the g values are ranging from 0.770 to 0.960. For g approaching unity, the R–P equation reduces to Langmuir isotherm. Generally, the adsorption of large adsorbate (dye molecules) renders a constant g lesser than 1 due to the obstruction of solid particles between the adsorbate and pores. Overall, the Langmuir and Redlich–Peterson models demonstrate a better fitting to the equilibrium data of MB adsorption, signifying a dominant single-layered adsorption of dye molecules onto a homogeneous surface of activated carbons.

Fig. 9 shows the effect of pH on the removal of MB by AC10-2. In general, the adsorption of MB is somewhat pH-independent with no obvious pattern of increasing or decreasing removal percentage with increasing solution pH from 3.0 to 10.3. The average removal is about 67.6%. However, an increasing adsorption could be observed at pH 6.3 (solution pH unadjusted) to pH 10.3. At pH 10.3, the solution pH is greater than pH_{PZC} of AC10-2, given the condition where the dye removal is 80.6% due to surface deprotonation as a result of hydroxyl anions governing the surface, hence favoring the cationic dye adsorption.

Table 4
Isotherm constants

Isotherm models	AC10-2	AC10-5	AC9-2	AC9-5	AC9-8
Q_{exp} (mg/g)	130	68.1	47.5	135	91.6
Langmuir model					
Q_m (mg/g)	132	70.7	46.5	128	86
b (L/mg)	0.320	0.204	0.549	0.946	1.750
SSE	892	178	293	2962	1558
R^2	0.946	0.989	0.925	0.836	0.849
Freundlich model					
K_f ((mg/g)(L/mg)$^{1/n}$)	42.7	36.1	21.4	56.7	65.3
n	3.51	7.16	5.38	4.44	14.4
SSE	2,299	189	365	4,496	1,405
R^2	0.867	0.987	0.877	0.754	0.864
Redlich–Peterson model					
K	47.2	19.5	33.3	163	115,182
a	0.416	0.340	0.886	1.61	17,645
g	0.960	0.956	0.948	0.933	0.931
SSE	866	175	286	2,812	1,406
R^2	0.948	0.990	0.922	0.845	0.864

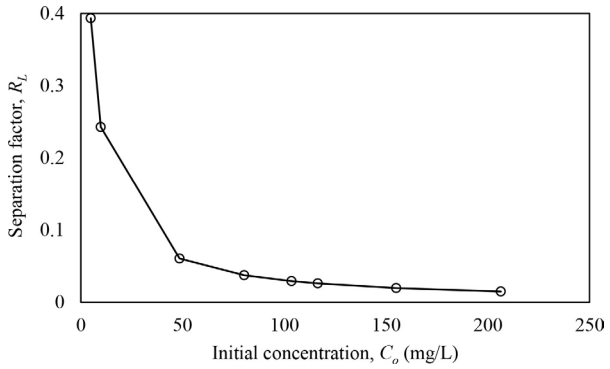

Fig. 8. Effect of initial concentration of methylene blue on separation factor, R_L of AC10-2.

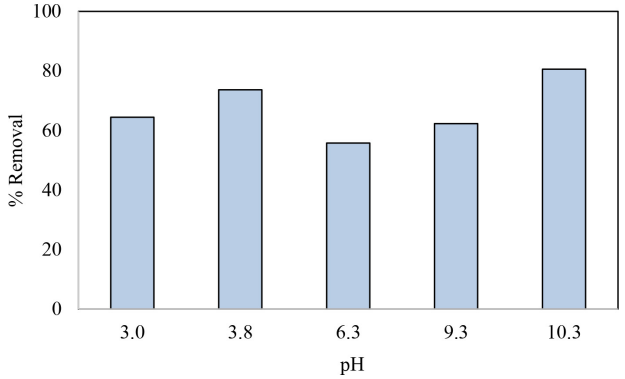

Fig. 9. Effect of pH on the removal of methylene blue onto AC10-2 (C_o = 20 mg/L).

3.3. Adsorption kinetics

Fig. 10 shows the rate of MB adsorption by AC9-5 and AC10-2. Both activated carbons display similar pattern of adsorption kinetics at different concentrations, owing to their comparable specific surface area. The adsorption of MB increases with time, while the time taken to reach equilibrium becomes longer when the initial concentration increases due to the decreasing number of vacant sites, hence declining the rate of adsorption.

Table 5 shows the constants of kinetic models. The fitting of kinetics data suggests that the rate of adsorption is better represented by the pseudo-second-order model. It is supported by the close agreement between the experimental Q_e and that from the pseudo-second-order model. From Table 5, the pseudo-second-order rate of constant, k_2 of AC10-2 and AC9-5 displays a decreasing trend with increasing dye concentration. The increase in concentration decreases the number of available (vacant) active sites, consequently decreasing the adsorption rate and rate constant [42].

Fig. 11 represents the intraparticle diffusion model for methylene blue adsorption onto AC10-2, which explains that the pore diffusion is not the sole rate-limiting step because the intercept did not pass through origin. The thickness of boundary layer can be determined by the c value in Eq. (8). A larger c suggests a better influence of film diffusion in the rate-limiting step. The trend of this model for all concentrations studied is identical. In the beginning, the adsorption demonstrates a dramatical increase signifying a strong attraction between dye molecules and the outer surface of activated carbon. Then, it is followed by a steady increase which indicates the pore adsorption. Lastly, a slow adsorption signifies the pore diffusion, and levelling-off to achieve the equilibrium state [43].

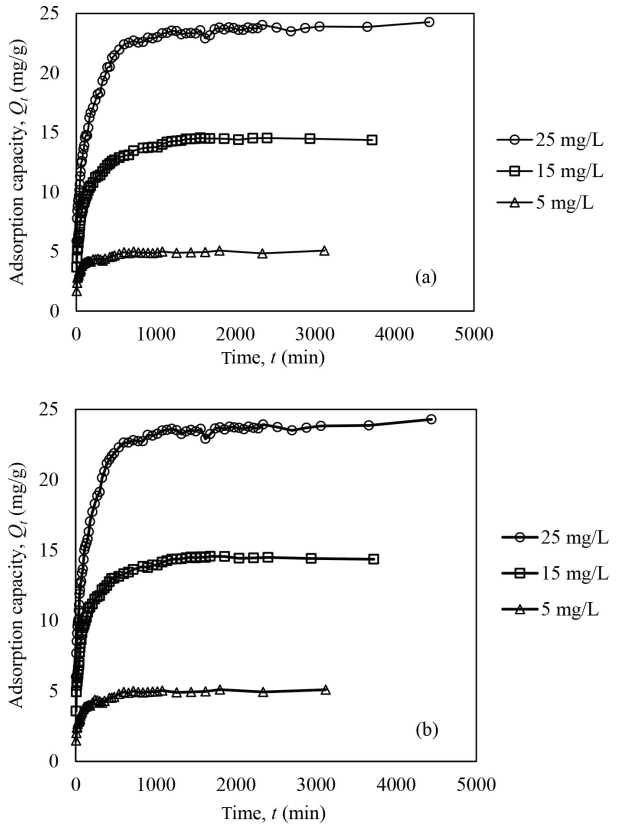

Fig. 10. Adsorption kinetics of methylene blue onto (a) AC9-5 and (b) AC10-2.

3.4. Adsorption thermodynamics

Fig. 12 shows the van't Hoff plot of AC10-2 at different concentrations. Generally, increasing the process temperature has resulted in the increase of equilibrium constant. It indicates that a greater capacity of equilibrium could be achieved at higher temperature. A greater equilibrium capacity is influenced by kinetic energy of MB molecules, whereby, in the presence of heat, the movement of molecules are energized, resulting in an increased adsorption rate due to the availability of active sites.

Table 6 summarizes the thermodynamic parameters of MB adsorption onto AC10-2. The entropy ($\Delta S°$) and enthalpy ($\Delta H°$) were determined from the slope and intercept of van't Hoff plot, respectively. The positive enthalpy represents an endothermic adsorption onto AC10-2, which could also be related to chemical adsorption mechanism [44].

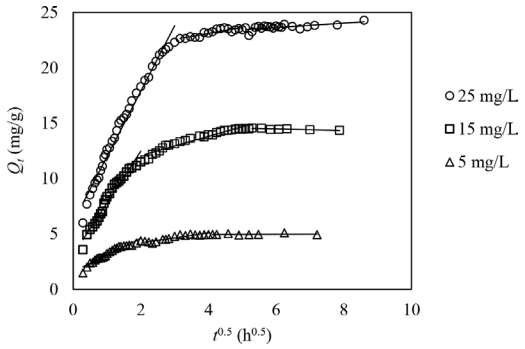

Fig. 11. Intraparticle diffusion of methylene blue adsorption by AC10-2 at different concentrations.

Table 5
Kinetic constants

Kinetic models	AC10-2			AC9-5		
	5 mg/L	15 mg/L	25 mg/L	5 mg/L	15 mg/L	25 mg/L
Experimental						
Q_e (mg/g)	4.96	14.5	24.3	4.97	14.4	24.3
Pseudo-first-order model						
Q_e (mg/g)	4.60	13.5	22.8	4.57	13.4	22.7
k_1 (min^{-1})	0.024	0.015	0.011	0.038	0.014	0.011
SSE	9.20	78.9	251	7.59	89.8	274
R^2	0.835	0.899	0.920	0.791	0.886	0.915
Pseudo-second-order model						
Q_e (mg/g)	4.90	14.4	24.0	4.90	14.3	24.1
k_2 (g/mg.min)	0.0078	0.0016	0.0008	0.0117	0.0015	0.0007
SSE	3.0	22.8	85.9	2.36	27.4	97.4
R^2	0.938	0.968	0.965	0.937	0.962	0.963
Intraparticle diffusion model						
k_d (mg/g $min^{0.5}$)	0.062	0.184	0.375	0.050	0.269	0.286
c (mg/g)	2.82	7.27	10.3	3.23	5.80	11.5
SSE	11.6	135	285	9.44	52.9	467
R^2	0.724	0.759	0.746	0.677	0.790	0.771

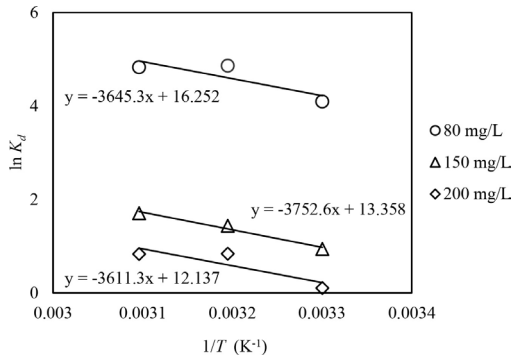

Fig. 12. Van't Hoff plot for methylene blue adsorption onto AC10-2 at different concentrations.

Table 6
Thermodynamic parameters of methylene blue adsorption onto AC10-2

C_o (mg/L)	$\Delta G°$(kJ/mol)			$\Delta H°$ (kJ/mol)	$\Delta S°$ (J/mol K)
	30°C	40°C	50°C		
80	–10.32	–12.67	–12.98	30.3	135
150	–2.37	–3.74	–4.58	31.2	111
200	–0.26	–2.18	–2.24	30.0	101

From Table 6, a greater adsorption capacity at higher temperature suggests that the adsorption activity is energized, as indicated by the positive $\Delta H°$. On the other hand, the negative $\Delta G°$ indicates that the adsorption of methylene blue is attainable, spontaneous and encouraging by thermodynamics. However, the $\Delta G°$ values are gradually approaching positive zero at lower temperature and higher concentration, indicating a non-spontaneity and a controlled adsorption activity. Under such conditions, the adsorption activity would require additional energy source to encourage spontaneity. At higher concentration, the movement of MB molecules to the surface of activated carbon would be delimited by the 'overly-packed' molecules [40]. During adsorption, the irregular randomness increased in the composition of adsorbent solution as indicated by the positive $\Delta S°$. This study recorded a decreasing trend of $\Delta S°$, with increasing dye concentration. It indicates a less-favorable endothermic process when the randomized movements of molecules are restricted. The $\Delta S°$ is directly influenced by the ability of molecules to move, whereby at higher concentration, the movement of molecules are impeded, resulting in a lower $\Delta S°$. Meanwhile, the $\Delta H°$ is directly affected by the frequency of adsorbate collision, generating a greater kinetic energy, driving a lower dependency for heat from the outside source, thus, resulting in a higher $\Delta H°$. The spontaneous and endothermic nature of adsorption have been reported in a number of studies [45,46].

The pyrolysis tyre powder–based activated carbon (AC10-2, S_{BET} = 243 m^2/g) displayed a promising prospective as dye adsorbent candidate for wastewater treatment. In relation to the recent studies on MB adsorption, H_3PO_4-activated shrimp shell (S_{BET} = 560.6 m^2/g) exhibits a capacity of 826 mg/g (b = 0.7908 L/mg), which increases with pH and temperature [47]. Li et al. [48] reported a 733 mg/g (b = 1.92 L/mg) capacity onto activated carbon derived from loofah sponge (S_{BET} = 733 m^2/g), which also increases with pH and temperature [48]. The karanj fruit hulls-based activated carbon shows a capacity of 154.8 mg/g, which increases with temperature but the solution pH does not offer significant change on the adsorption [30]. The AC10-2 (Q_m = 132 mg/g) from this work exhibits comparable findings, although the adsorption capacity is somewhat lesser as a result of low surface area. Hence, the post-treatment strategies are recommended to improve the inherent properties of activated carbon for a better performance in adsorption.

4. Conclusion

Activated carbons were synthesized from pyrolysis tyre powder by CO_2 activation at different activating times and temperatures. Activated carbon prepared at 1,000°C for 2 h (AC10-2) shows a higher surface area of 237 m^2/g, and a greater methylene blue adsorption of 132 mg/g. The equilibrium data fitted well with Langmuir and Redlich–Peterson models, implying a monolayer adsorption onto a homogeneous activated carbon surface. AC10-2 displays a somewhat pH independent adsorption behavior with varying solution pH. However, an increasing pattern is evident from pH 6.3 to pH 10.3, where the removal increases from 55.8% to 80.6%. The adsorption mechanism could be described as chemical adsorption in which film diffusion is probably the rate-controlling step. Also, the adsorption of methylene blue is endothermic and spontaneous in nature with increasing temperature.

Acknowledgment

The authors acknowledged the financial aid of UTM Tier-1 Research University Grant No. 18H50.

References

[1] N. Bensalah, M. Alfaro, C. Martínez-Huitle, Electrochemical treatment of synthetic wastewaters containing alphazurine A dye, Chem. Eng. J., 149 (2009) 348–352.
[2] S. Dawood, T.K. Sen, C. Phan, Synthesis and characterization of novel activated carbon from waste biomass pine cone and its application in the removal of congo red dye from aqueous solution by adsorption, Water Air Soil Pollut., 225 (2014) 1–16.
[3] D. Wróbel, A. Boguta, R.M. Ion, Mixtures of synthetic organic dyes in a photoelectrochemical cell, J. Photochem. Photobiol. Chem., 138 (2001) 7–22.
[4] J.W. Lee, S.P. Choi, R. Thiruvenkatachari, W.G. Shim, H. Moon, Evaluation of the performance of adsorption and coagulation processes for the maximum removal of reactive dyes, Dyes Pigm., 69 (2006) 196–203.
[5] C.K. Lee, K.S. Low, P.Y. Gan, Removal of some organic dyes by acid treat spent bleaching earth, Environ. Technol., 20 (1999) 99–104.
[6] A.B. Albadarin, M.N. Collins, M. Naushad, S. Shirazian, G. Walker, C. Mangwandi, Activated lignin-chitosan extruded blends for efficient adsorption of methylene blue, Chem. Eng. J., 307 (2017) 264–272.
[7] G. Sharma, Mu. Naushad, A. Kumar, S. Rana, S. Sharma, A. Bhatnagar, F.J. Stadler, A.A. Ghfar, M.R. Khan, Efficient removal of coomassie brilliant blue R-250 dye using starch/poly(alginic acid-cl-acrylamide) nanohydrogel, Process Saf. Environ., 109 (2017) 301–310.
[8] M.T. Yagub, T.K. Sen, S. Afroze, H.M. Ang, Dye and its removal from aqueous solution by adsorption: a review, Adv. Colloid Interface Sci., 209 (2014) 172–184.

[9] S. Rangabhashiyam, N. Anu, N. Selvaraju, Sequestration of dye from textile industry wastewater using agricultural waste products as adsorbents, J. Environ. Chem. Eng., 1 (2013) 629–641.
[10] G. Crini, Non-conventional low-cost adsorbents for dye removal: a review, Bioresour. Technol., 97 (2006) 1061–1085.
[11] B. Ismail, S.T. Hussain, S. Akram, Adsorption of methylene blue onto spinel magnesium aluminate nanoparticles: adsorption isotherms, kinetic and thermodynamic studies, Chem. Eng. J., 219 (2013) 395–402.
[12] R.A. Reza, M. Ahmaruzzaman, Comparative study of waste derived adsorbents for sequestering methylene blue from aquatic environment, J. Environ. Chem. Eng., 3 (2015) 395–404.
[13] V.K. Jha, K. Subedi, Preparation of activated carbons from waste tire, Nepal Chem. Soc., 27 (2011) 19–25.
[14] F. Ahmad, W.M.A.W. Daud, M.A. Ahmad, R. Radzi, Cocoa (*Theobroma cacao*) shell-based activated carbon by CO_2 activation in removing of Cationic dye from aqueous solution: kinetics and equilibrium studies, Chem. Eng. Res. Des., 90 (2012) 1480–1490.
[15] A. Rowhani, T. Rainey, Scrap tyre management pathways and their use as a fuel - a review, Energies, 9 (2016) 1–26.
[16] A. Turer, Recycling of Scrap Tires, In: D. Achilias, Material Recycling - Trends and Perspectives, InTech Open, Rijeka, 2012, pp. 195–212.
[17] J. Downard, A. Singh, R. Bullard, T. Jayarathne, C.M. Rathnayake, D.L. Simmons, B.R. Wels, S.N. Spak, T. Peters, D. Beardsley, C.O. Stainer, E.A. Stone, Uncontrolled combustion of shredded tires in a landfill - Part 1: characterization of gaseous and particulate emissions, Atmos. Environ., 104 (2015) 195–204.
[18] A. Singh, S.N. Spak, E.A. Stone, J. Downard, R. Bullard, M. Pooley, P.A. Kostle, M.W. Mainprize, M.D. Wichman, T.M. Peters, D. Beardsley, C.O. Stainer, Uncontrolled combustion of shredded tires in a landfill - Part 2: population exposure, public health response, and an air quality index for urban fires, Atmos. Environ., 104 (2015) 273–283.
[19] V. Torretta, E.C. Rada, M. Ragazzi, E. Trulli, I.A. Istrate, L.I. Cioca, Treatment and disposal of tyres: Two EU approaches. A review, Waste Manage., 45 (2015) 152–160.
[20] I. Hita, M. Arabiourrutia, M. Olazar, J. Bilbao, J.M. Arandes, P. Castano, Opportunities and barriers for producing high quality fuels from the pyrolysis of scrap tires, Renew. Sustain. Energy Rev., 56 (2016) 745–759.
[21] M.A.A. Zaini, T. Chiew-Ngiik, M.J. Kamaruddin, S.H. Mohd-Setapar, M.A. Che-Yunus, Zinc chloride-activated waste carbon powder for decolourization of methylene blue, Jurnal Teknologi Sci. Eng., 67 (2014) 37–44.
[22] F.A. López, T.A. Centeno, O. Rodríguez, F.J. Alguacil, Preparation and characterization of activated carbon from the char produced in the thermolysis of granulated scrap tyres, J. Air Waste Manage. Assoc., 63 (2013) 534–544.
[23] K.C. Bedin, A.C. Martins, A.L. Cazetta, O. Pezoti, V.C. Almeida, KOH-activated carbon prepared from sucrose spherical carbon: adsorption equilibrium, kinetic and thermodynamic studies for methylene blue removal, Chem. Eng. J., 286 (2016) 476–484.
[24] I. Langmuir, The adsorption of gases on plane surfaces of glass, mica and platinum, J. Am. Chem. Soc., 40 (1918) 1361–1403.
[25] O. Pezoti, A.L. Cazetta, I.P.A.F. Souza, K.C. Bedin, A.C. Martins, T.L. Silva, V.C. Almeida, Adsorption studies of methylene blue onto $ZnCl_2$-activated carbon produced from buriti shells (*Mauritia flexuosa* L.), J. Ind. Eng. Chem., 20 (2014) 4401–4407.
[26] P. Jutakridsada, C. Prajaksud, L.K. Aruk, S. Theerakulpisut, K. Kamwilaisak, Adsorption characteristics of activated carbon preparedfrom spent ground coffee, Clean Tech. Environ. Policy, 18 (2016) 639–645.
[27] M. Naushad, T. Ahamad, B.M. Al-Maswari, A.A. Alqadami, S.M. Alshehri, Nickel ferrite bearing nitrogen-doped mesoporous carbon as efficient adsorbent for the removal of highly toxic metal ion from aqueous medium, Chem. Eng. J., 330 (2017) 1351–1360.
[28] E.G. Sogut, N. Caliskan, Isotherm and kinetic studies of Pb(II) adsorption on raw and modified diatomite by using non-linear regression method, Fresen. Environ. Bull., 26 (2017) 2721–2729.
[29] B. Acevedo, C. Barriocanal, I. Lupul, G. Gryglewicz, Properties and performance of mesoporous activated carbons from scrap tyres, bituminous wastes and coal, Fuel, 151 (2015) 83–90.
[30] M.A. Islam, S. Sabar, A. Benhouria, W.A. Khanday, M. Asif, B.H. Hameed, Nanoporous activated carbon prepared from karanj (*Pongamia pinnata*) fruit hulls for methylene blue adsorption, J. Taiwan Inst. Chem. Eng., 74 (2017) 96–104.
[31] T. Maneerung, J. Liew, Y. Dai, S. Kawi, C. Chong, C.H. Wang, Activated carbon derived from carbon residue from biomass gasification and its application for dye adsorption: kinetics, isotherms and thermodynamic studies, Bioresour. Technol., 200 (2016) 350–359.
[32] J. Haydary, Z. Koreňová, Ľ. Jelemenský, J. Markoš, Thermal decomposition of waste polymers, Thermophysics, (2008) 62–68.
[33] E. Kwon, M.J. Castaldi, Investigation of Thermo-Gravimetric Analysis (TGA) on Waste Tires and Chemical Analysis Including Light Hydrocarbons, Substituted Aromatics, and Polycyclic Aromatic hydrocarbon (PAH), 15th North American Waste to Energy Conference, 2007, pp. 183–190.
[34] C.F. Chang, C.Y. Chang, W.T. Tsaiy, Effects of burn-off and activation temperature on preparation of activated carbon from corn cob agrowaste by CO_2 and steam, J. Colloid Interface Sci., 232 (2000) 45–49.
[35] H. Hadi, K.Y. Yeung, J. Guo, H. Wang, G. McKay, Sustainable development of tyre char-based activated carbons with different textural properties for value-added applications, J. Environ. Manage., 170 (2016) 1–7.
[36] A.H. Lu, F. Schuth, Nanocasting: a versatile strategy for creating nanostructured porous materials, Adv. Mater., 18 (2006) 1793–1805.
[37] G. Leofanti, M. Padovan, G. Tozzola, B. Venturelli, Surface area and pore texture of catalysts, Catal. Today, 41 (1998) 207–219.
[38] X. Colom, A. Faliq, K. Formela, J. Canavate, FTIR spectroscopic and thermogravimetric characterization of ground tyre rubber devulcanized by microwave treatment, Polym. Test., 52 (2016) 200–208.
[39] S. Galvagno, S. Casu, M. Martino, E.D. Palma, S. Portofino, Thermal and kinetic study of tyre waste pyrolysis via tg-ftir-ms analysis, J. Therm. Anal. Calorim., 88 (2007) 507–514.
[40] S.H. Tang, M.A.A. Zaini, Malachite green adsorption by potassium salts-activated carbons derived from textile sludge: equilibrium, kinetics and thermodynamics studies, Asia-Pac. J. Chem. Eng., 12 (2016) 159–172.
[41] O.J. Redlich, D.L. Peterson, A useful adsorption isotherm, J. Phy. Chem., 63 (1959) 1024–1026.
[42] M.A.A. Zaini, N. Alias, M.A. Che-Yunus, Bio-polishing sludge adsorbents for dye removal, Pol. J. Chem. Technol., 18 (2016) 15–21.
[43] L.L. Zhi, M.A.A. Zaini, Adsorption properties of cationic rhodamine B dye onto metals chloride-activated castor bean residue carbons, Water Sci. Technol., 75 (2017) 864–880.
[44] H.N. Tran, S.J. You, A.H. Bandegharaei, H.P. Chao, Mistakes and inconsistencies regarding adsorption of contaminants from aqueous solutions: a critical review, Water Res., 120 (2017) 88–116.
[45] Mu. Naushad, S. Vasudevan, G. Sharma, A. Kumar, Z.A. ALOthman, Adsorption kinetics, isotherms, and thermodynamic studies for Hg^{2+} adsorption from aqueous medium using alizarin red-S-loaded amberlite IRA-400 resin, Desal. Wat. Treat., 57 (2016) 18551–18559.
[46] Mu. Naushad, G. Sharma, A. Kumar, S. Sharma, A.A. Ghfar, A. Bhatnagar, F.J. Stadler, M.R. Khan, Efficient removal of toxic phosphate anions from aqueous environment using pectin based quaternary amino anion exchanger, Int. J. Biol. Macromol., 106 (2018) 1–10.
[47] X. Liu, C. He, X. Yu, Y. Bai, L. Ye, B. Wang, L. Zhang, Net-like porous activated carbon materials from shrimp shell by solution-processed carbonization and H_3PO_4 activation for methylene blue adsorption, Powder Technol., 326 (2018) 181–189.
[48] Z. Li, G. Wang, K. Zhai, C. He, Q. Li, P. Guo, Methylene blue adsorption from aqueous solution by loofah sponge-based porous carbons, Colloids Surf. A, 538 (2018) 28–35.